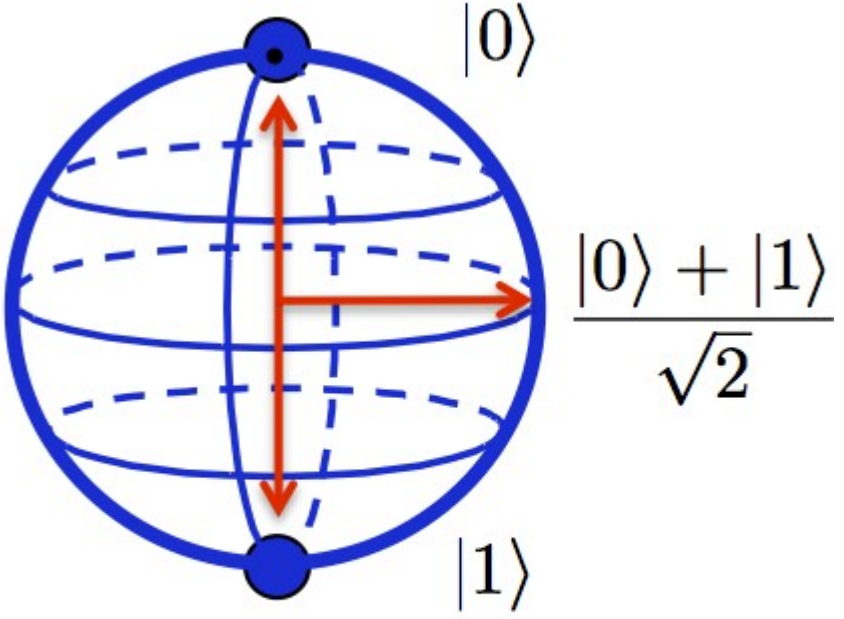

Classical Bit **Qubit**

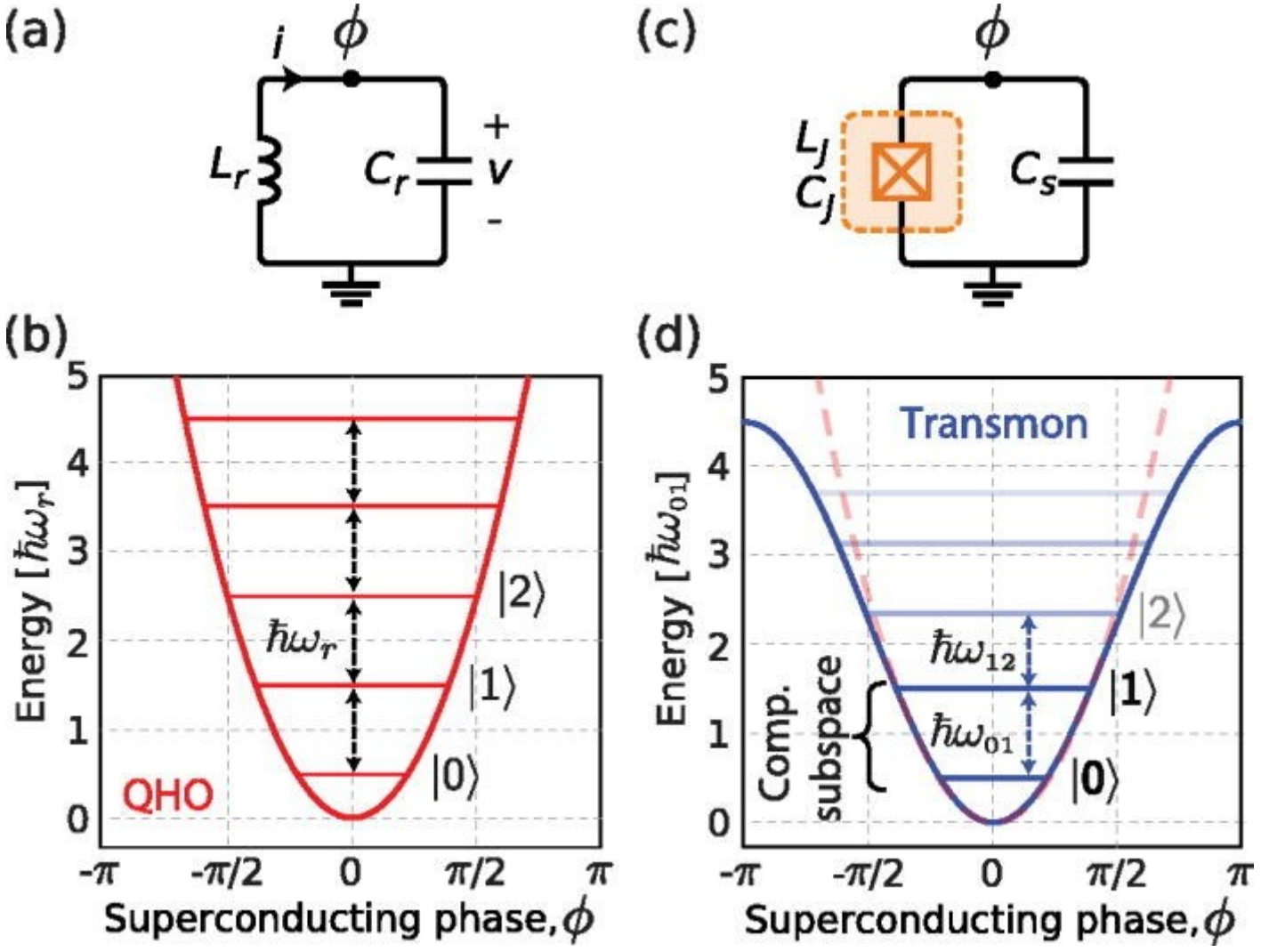
(a)
i
ϕ
L_r
C_r
+
v
-
(c)
ϕ
L_J
C_J
C_s
(b)
Energy [$\hbar\omega_r$]
5
4
3
2
1
0
$\hbar\omega_r$
|2⟩
|1⟩
|0⟩
QHO
-π
-π/2
0
π/2
π
Superconducting phase, ϕ
(d)
Energy [$\hbar\omega_{01}$]
Transmon
$\hbar\omega_{12}$
$\hbar\omega_{01}$
Comp. subspace
|2⟩
|1⟩
|0⟩
Superconducting phase, ϕ

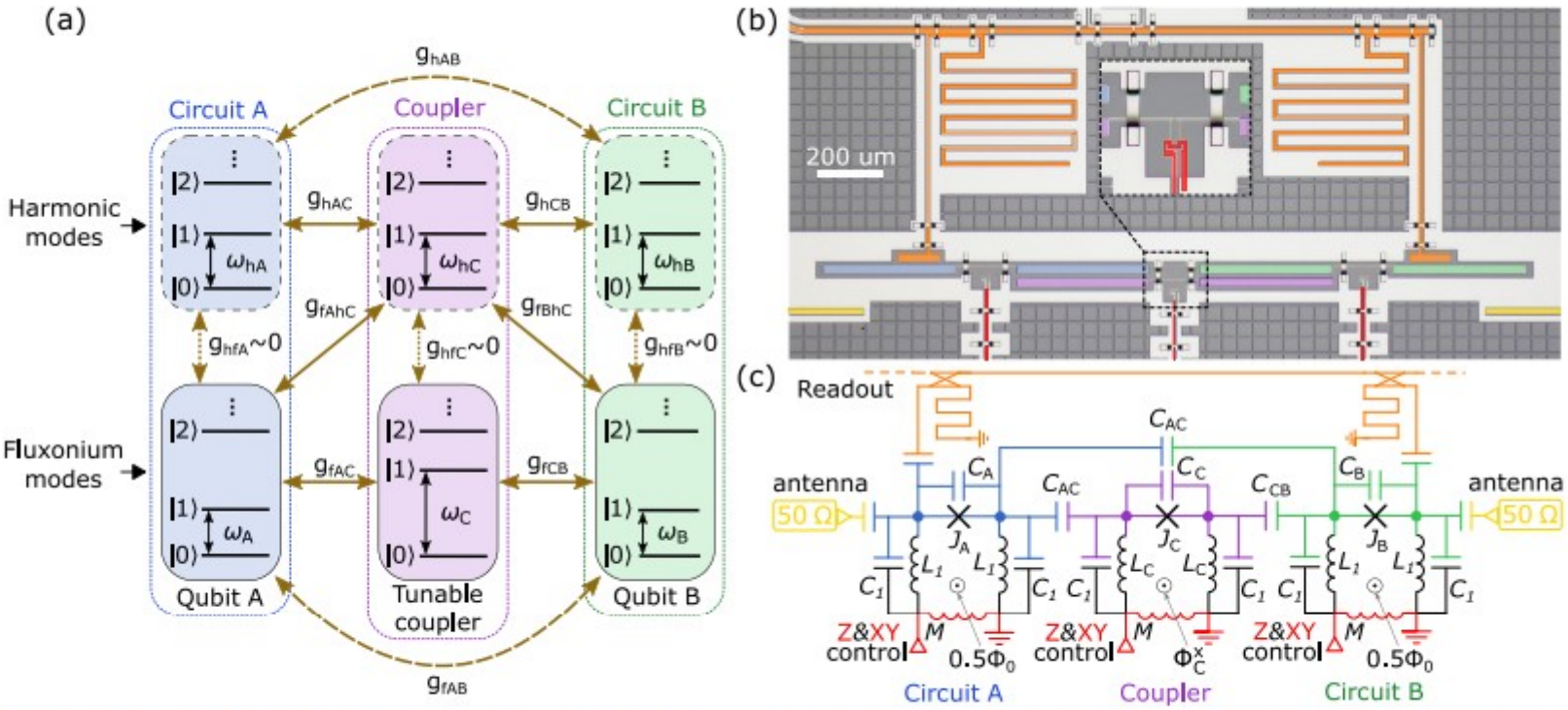

Fig. 1 The fluxonium-based two-qubit quantum processor. a Schematic diagram of an interacting three-body system. **b** Experimental realization of three capacitively coupled fluxonium-like qubits fabricated on a silicon substrate. **c** Circuit schematic. In **b**, false colors (blue, purple, green, orange, yellow, and red) are used to indicate the corresponding circuit components in **d**. 50 Ω terminators are installed at the 10 mK stage of the dilution refrigerator and used for qubits initialization (see Supplementary Fig. 1 for details).

As described in ref. [28], after eliminating the coupler degrees of freedom and harmonic modes (h_A, h_B), our two-qubit processor obeys the effective low-energy Hamiltonian:

$$\hat{H}_{\mathrm{eff}}/\hbar = -\frac{1}{2}\omega_A\sigma_A^z - \frac{1}{2}\omega_B\sigma_B^z + g_{xx}\sigma_A^x\sigma_B^x + \frac{1}{4}\zeta_{zz}\sigma_A^z\sigma_B^z. \quad (2)$$

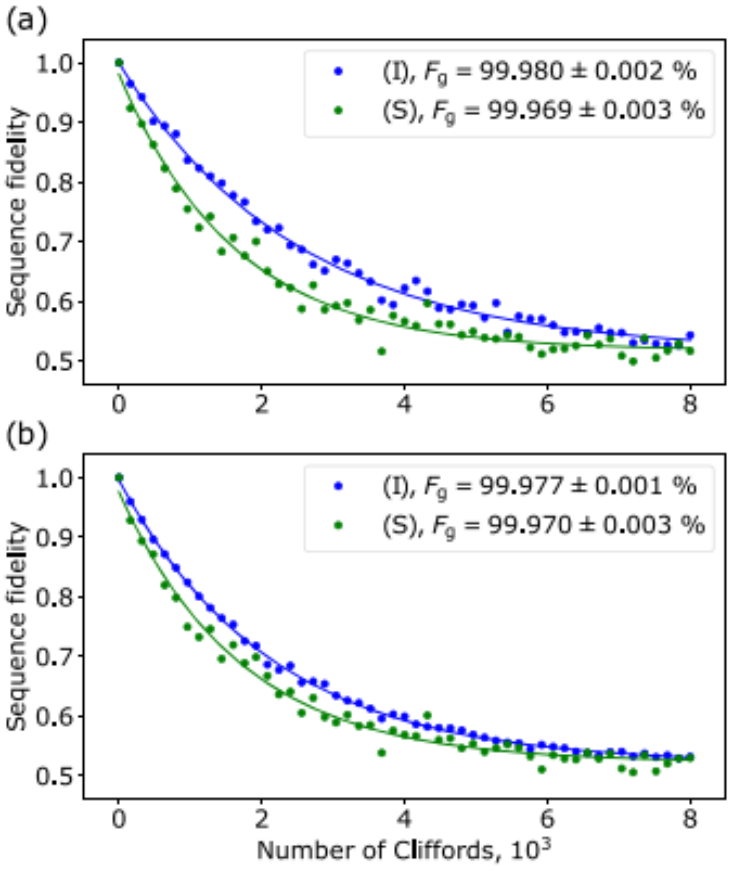

Fig. 2 Experimental results of randomized benchmarking for single-qubit gates on qubit A and qubit B. a Measurement data of single-qubit RB for qubit A. **b** Measurement data of single-qubit RB for qubit B. "I" denotes the isolated application of single-qubit Cliffords and isolated qubit readout. "S" denotes the simultaneous application of single-qubit Cliffords and joint-qubit readout. Error estimates for fidelity are obtained from the least square fit errors. The data were averaged over 20 random sequences for each

Two-qubit gates using a tunable coupler

Our two-qubit device allows to implement universal two-qubit gates from the fSim family[7,9], which describes the set of excitation number-preserving quantum logic operations on two qubits up to single-qubit phase rotations. Its matrix representation in the $|00\rangle$, $|01\rangle$, $|10\rangle$, $|11\rangle$ basis is given by:

$$\mathrm{fSim}(\theta,\varphi) = \begin{pmatrix} 1 & 0 & 0 & 0 \\ 0 & \cos\theta & -i\sin\theta & 0 \\ 0 & -i\sin\theta & \cos\theta & 0 \\ 0 & 0 & 0 & e^{-i\varphi} \end{pmatrix}, \tag{4}$$

where θ is the swap angle, and φ is the conditional phase.

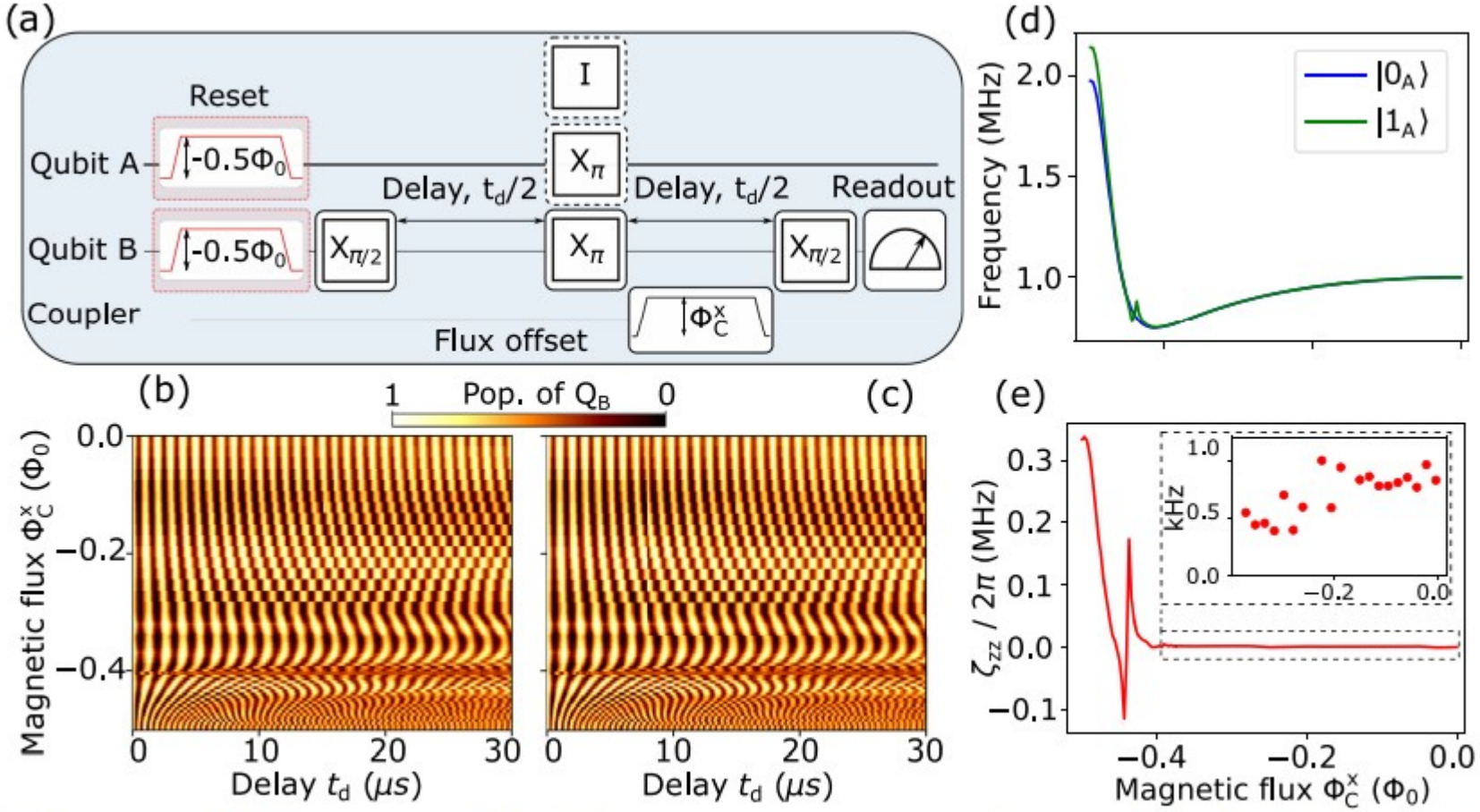

Fig. 3 Measurement of ZZ interaction strength ζ_{zz}. a Pulse sequence of an echo-type experiment on qubit B while initializing qubit A in its ground (preparation gate *I*) or exited (preparation gate X_π) state. The final $\pi/2$-pulse phase is modulated proportionally to the delay. **b** Qubit B

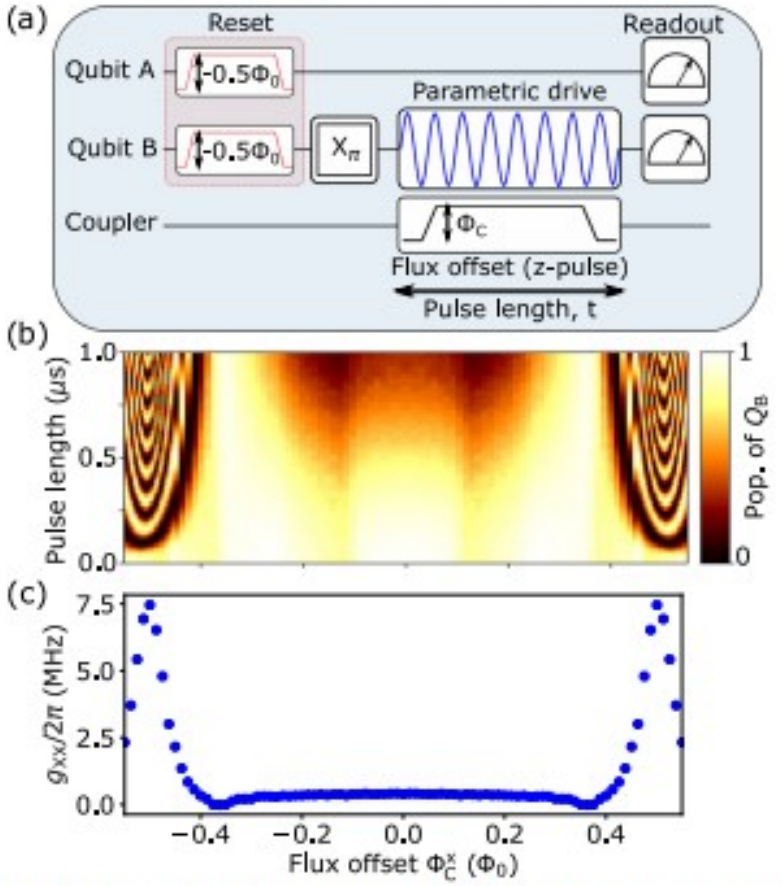

Fig. 4 Effective XX coupling strength as a function of coupler flux. **a** Pulse sequence to measure qubit-qubit coupling under modulation (qubit B tuned in resonance with qubit A) as a function of the coupler flux bias. **b** Experimental data for the energy exchange between $|10\rangle$ and $|01\rangle$, as a function of the magnetic flux in the coupler Φ_C^x. **c** The effective qubit-qubit coupling g_{xx} versus Φ_C^x.

Matrix Representation:

$$iSWAP = R_{XX+YY}\left(-\frac{\pi}{2}\right) = \exp\left(i\frac{\pi}{4}(X\otimes X + Y\otimes Y)\right) = \begin{pmatrix} 1 & 0 & 0 & 0 \\ 0 & 0 & i & 0 \\ 0 & i & 0 & 0 \\ 0 & 0 & 0 & 1 \end{pmatrix}$$

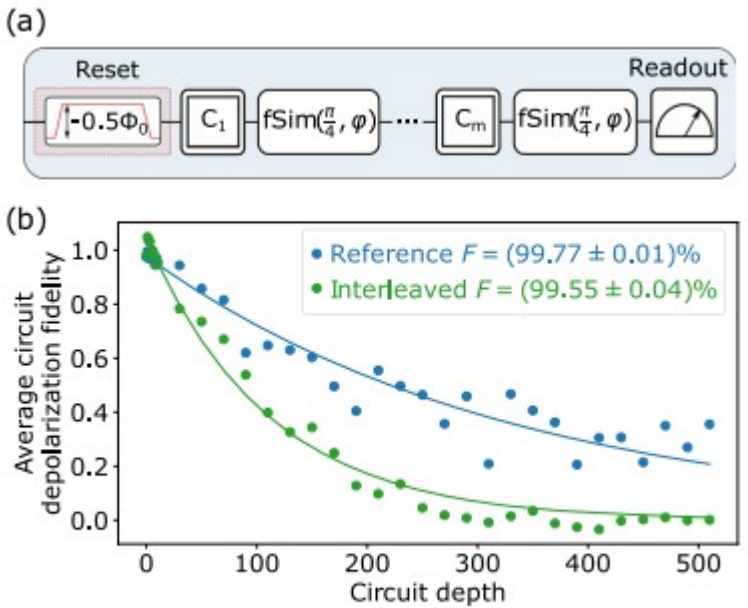

Fig. 5 Cross-entropy benchmarking (XEB) of the $\sqrt{\text{iSWAP}}$-like gate. a Pulse sequence for the XEB experiment. **b** Depolarization fidelity for the reference circuits and interleaved circuits.

Matrix representation:

$$CZ\ q_0, q_1 = I \otimes |0\rangle\langle 0| + Z \otimes |1\rangle\langle 1| = \begin{pmatrix} 1 & 0 & 0 & 0 \\ 0 & 1 & 0 & 0 \\ 0 & 0 & 1 & 0 \\ 0 & 0 & 0 & -1 \end{pmatrix}$$

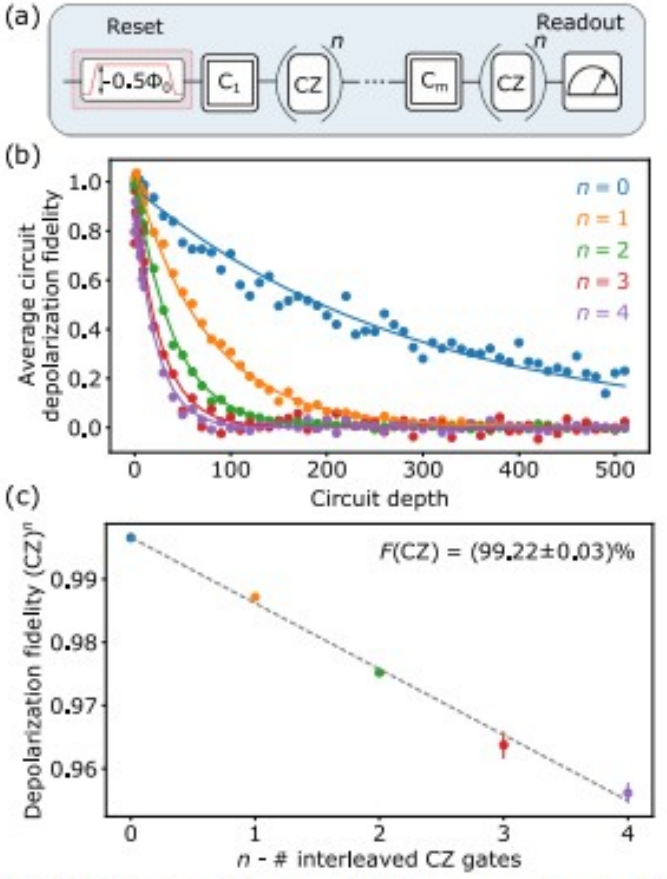

Fig. 7 XEB for the CZ gate. a Pulse sequence for the XEB experiment with the CZ gate. **b** XEB results of the CZ gate. We use a variable number of CZ gates (up to 4) (encoded in color) between the randomly chosen Clifford gates. For each circuit depth, we average over 100 sequences. **c** Fidelity of CZ^n versus n. Linear dependence indicates incoherent errors.

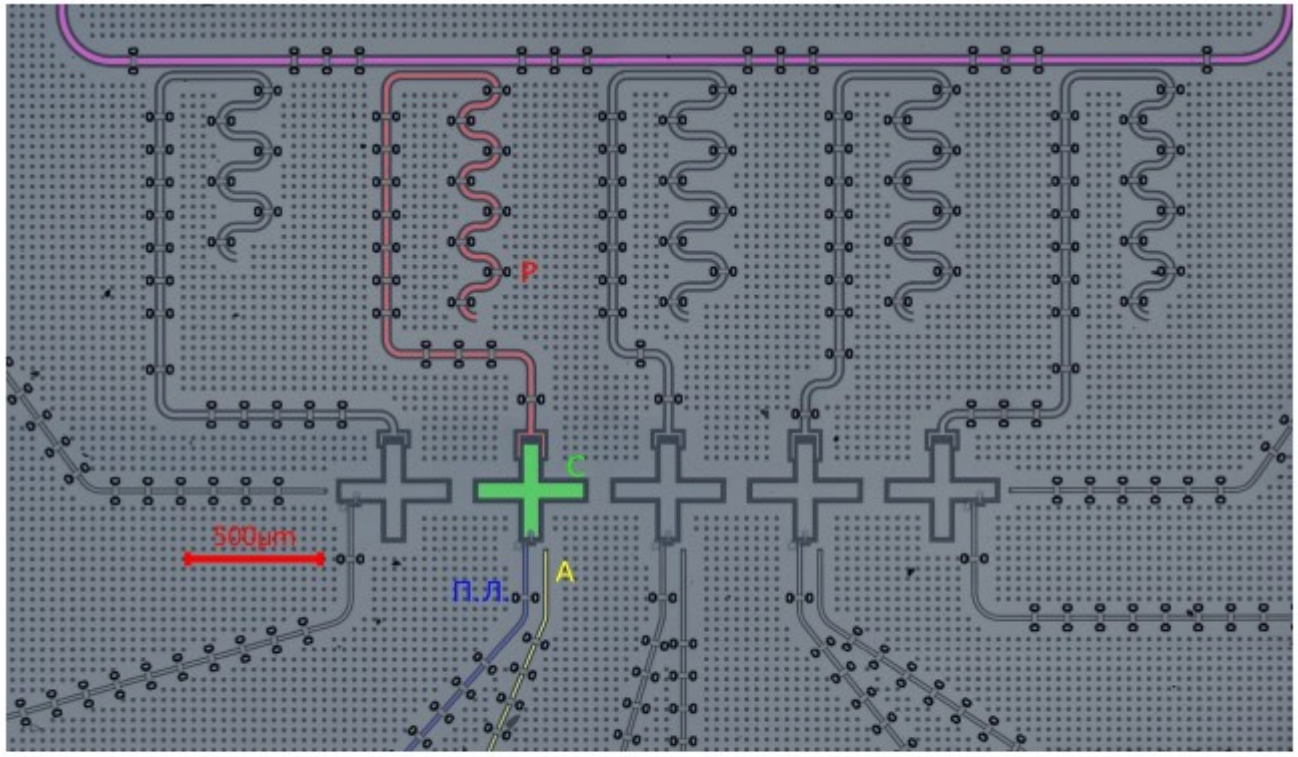

Рис. 1. *Фотография КИМС с оптического микроскопа (в ложном цвете). Микросхема реализует кубитов (емкость одного из них отмечена зеленым), связанных с резонаторами (красный) для индивидуального считывания. Каждый кубит снабжен управляющей потоковой линией и антенно для осуществления однокубитных операций (синий и желтый, соответственно).*

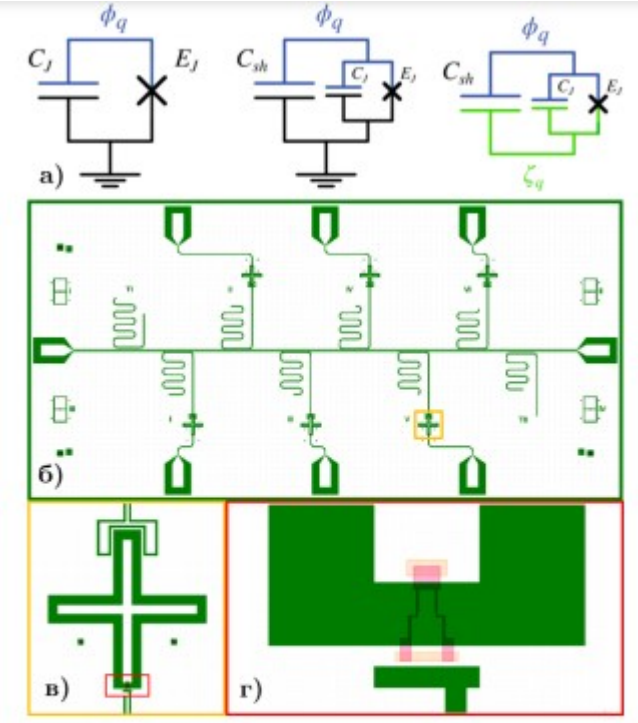

Рис.5. а) эквивалентные схемы кубитов (слева направо): зарядовый кубит, кубит-иксмон и двухостровковый трансмон; б) пример топологии планарного образца; в) вид конденсатора кубита-иксмона. г) сверхпроводящая петля (СКВИД) кубита-иксмона.

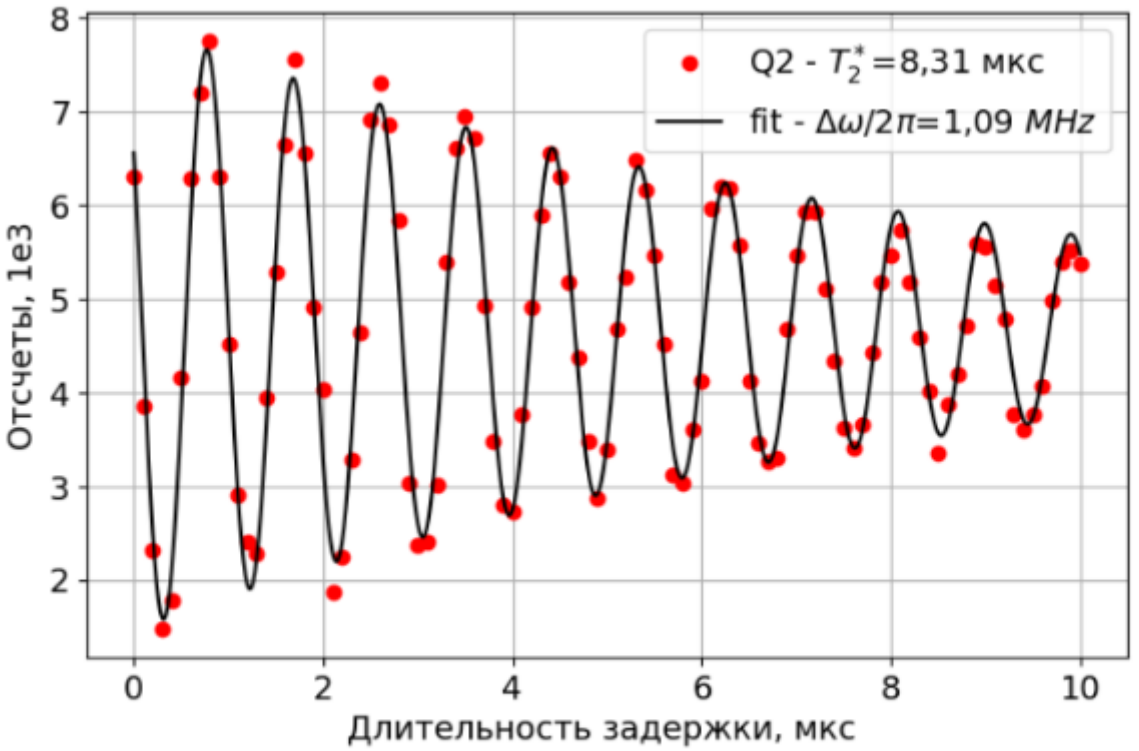

Рис. 3. *Зависимость когерентности кубита от времени измерения. Время когерентности, вычисленное путем аппроксимации данных, составляет 8.31 мкс.*

t1=0.025мкс